JOURNAL OF SPACECRAFT AND ROCKETS
Vol. 36, No. 5, September–October 1999

# Three-Dimensional Shock/Boundary-Layer Interaction Between a Rocket and a Booster

Yoshiharu Tanahashi,* Tsuyoshi Ohara,* and Yoshiaki Nakamura†
*Nagoya University, Nagoya 464-8603, Japan*

**A shock-tunnel experiment was conducted to examine the characteristics of three-dimensional flowfield on the surface of a rocket in the vicinity of the nose of a booster. In particular, attention was paid to the interaction of a boundary layer on the rocket surface with a bow shock generated by the booster. Three shapes of booster nose were employed to change the strength of the bow shock, that is, to vary the magnitudes of heat flux and pressure on the rocket surface: hemisphere, cone, and hemisphere-cone. Results indicate that in the case of the hemisphere booster nose the heat flux and pressure have complicated distributions with locally lower values just upstream of the major peaks because of strong interaction. This suggests that a separation bubble occurs with a secondary separation inside it, which was confirmed by oil-flow visualization. This phenomenon was not discernable in the other two cases because of weak interactions. In the comparison of heat flux and static-pressure distributions, the heat flux was affected by the interaction more widely in the circumferential direction than the pressure, which can be a three-dimensional effect. Quantitatively, more accurate data were acquired by using thin-film resistance thermometers than previously published data, which were measured by thin-skin thermocouples. From these data, a new correlation between heat flux and pressure with regard to their peak values was obtained, where the upstream flow is laminar and interaction region is turbulent.**

## Nomenclature

$c$ = specific heat of sensor base substrate, J/kg-K
$D$ = diameter of main body, m
$F$ = constant
$H$ = convective heat-transfer coefficient, W/m$^2$-K
$M$ = Mach number
$n$ = constant
$P$ = static pressure, Pa
$P_0$ = total pressure of wind tunnel, Pa
$\dot{q}$ = heat flux, W/m$^2$
$Re$ = Reynolds number
$T$ = rocket surface temperature change from the start of heating, K
$t$ = time from the start of heating of the rocket surface, s
$t_a$ = half of time-averaged period, s
$t_r$ = time at which rocket surface static pressure takes the value of 4 MPa, s
$X$ = axial coordinate along main body center line with $X = 0$ at the shoulder of booster, m
$Y$ = radial coordinate on the vertical plane including the booster axis, m
$\theta$ = circumferential angle of main body from $Y$ axis, deg
$\kappa$ = thermal conductivity of sensor base substrate, J/m-s-K
$\rho$ = density of sensor base substrate, kg/m$^3$
$\tau$ = time during time-averaged period, s

*Subscripts*

aw = adiabatic wall
$i$ = interaction
$k$ = constant ($k = 1, 2, 3, \ldots, r$)
$l$ = laminar
pk = peak
$r$ = the number of time interval steps ($r = 1, 2, 3, \ldots$)
$t$ = turbulent
$u$ = undisturbed
$w$ = wall (rocket surface)

## Introduction

RECENTLY, new versions of supersonic and hypersonic flight vehicles such as rocket, supersonic transport, and spaceplane have been proposed worldwide. In the development of those vehicles, one often encounters shock/boundary-layer interaction problems caused by shock waves generated by the different parts of the vehicles.

Over the past four decades many studies have been devoted to examining these interactions by reviewing the distributions of aerodynamic heating and pressure for two-dimensional and three-dimensional flows both in laminar and turbulent boundary-layer states.[1–11] However, detailed flow mechanisms especially in the three-dimensional interactions have not been made clear yet because of the complexity. Correlation between convective heat-transfer coefficient and static pressure with respect to their peak values in the interaction region also has not been fully achieved because of errors in the measurement of heat flux. The correlation data that have been reported by most researchers were measured with thin-skin thermocouples. This measurement method causes relatively large data error because of thermal conduction, especially at the location of high temperature gradient along the surface.

In the present study heat flux and static-pressure data were measured experimentally for a rocket-booster configuration, where three nose shapes were employed for the booster. To help the understanding of the complicated distributions of heat flux and static pressure over the body surface, the flowfield was also visualized by the oil-flow method and schlieren photography. To reduce the error in the measurement of heat flux, thin-film resistance thermometers were used in this study. This method has smaller thermal conduction error than thin-skin thermocouples.

In the results and discussion we discuss detailed flow mechanisms in the interacted region, which are different between the three shapes of the booster nose. In addition, a three-dimensional effect is noted by comparing the transverse changes in heat flux and static pressure. In the case of the three-dimensional interaction flow, the main body model is curved in the transverse direction. Heat flux depends not only on static pressure outside the boundary layer but also on the temperature gradient inside it. This characteristic produces three-dimensional effects in the interaction that is of interest in this study.

Presented as Paper 97-2572 at the AIAA 32nd Thermophysics Conference, Atlanta, GA, 23–25 June 1997; received 31 August 1998; revision received 10 February 1999; accepted for publication 20 February 1999. 

*Graduate Student, School of Engineering.
†Professor, Department of Aerospace Engineering. Member AIAA.

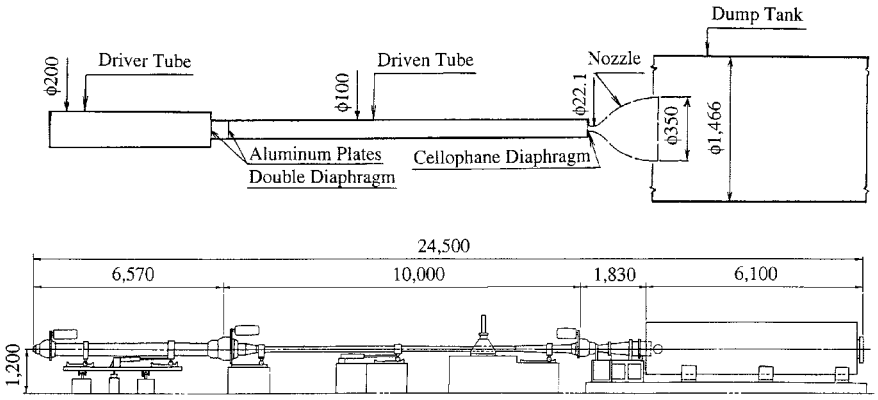


**Fig. 1 Shock tunnel at Nagoya University.**

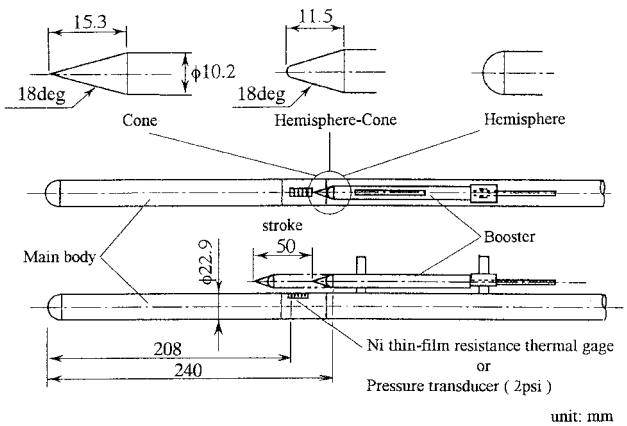


**Fig. 2 Model configuration.**

Finally, for the aerothermal design we discuss a new correlation between heat-transfer coefficient and static pressure with regard to the ratio of a peak value to the corresponding undisturbed value in experimental data.

## Facilities and Models

The shock tunnel we used has a contoured nozzle whose exit diameter is 350 mm, and the core flow diameter is about 200 mm (Fig. 1). This tunnel uses air as the working gas and can achieve a Mach number of 8.1. The freestream Reynolds number based on half a distance of square root of the nozzle exit area, 155 mm, is about $0.89 \times 10^6$. The static pressure of the freestream is about 0.38 kPa, and the static temperature is about 67 K.

A rocket model with a booster is shown in Fig. 2. The booster is designed to be traversable in the model axis direction to change the relative position of the booster with respect to the main body. The distance between the rocket and the booster is fixed at 5 mm to keep the booster out of the boundary layer on the main body. In the interaction region under consideration, several sensors to measure heat flux and static pressure are mounted on the rocket surface. The distance from the rocket nose to the head of the foremost sensor is 208 mm. Moreover, the part of the main body where the sensors are installed can be rotated about the main body axis within the range of 0–90 deg. Thus, the data of heat flux and static pressure can be collected at many locations with a limited number of sensors. Thin-film resistance thermometers are used for the measurement of temperatures on the rocket surface, and pressure transducers with a capacity of 2 psi are mounted about 10 mm in depth from the surface to measure static pressure. To change the strength of the bow shock, three geometrical shapes of the booster nose were considered: hemisphere, cone, and hemisphere-cone. The hemisphere-cone and the cone have the same vertex angle. To specify the location at which data were measured, the coordinate system employed here is shown in Fig. 3.

## Data Reduction

First, the heat flux is calculated based on measured temperature data by using the following equation[12]:

$$\dot{q}_{t=t_r} = 2\sqrt{\frac{\rho c \kappa}{\pi}} \sum_{k=1}^{r} \frac{T(t_k) - T(t_{k-1})}{(t_r - t_k)^{\frac{1}{2}} + (t_r - t_{k-1})^{\frac{1}{2}}} \tag{1}$$

where $t = 0$ to $t_k (< t_r)$. By making use of this value for $\dot{q}$, we obtain the heat-transfer coefficient

$$H = \frac{\dot{q}}{T_{\mathrm{aw}} - T_w} \tag{2}$$

where $T_{\mathrm{aw}}$ is the adiabatic wall temperature at a measured point on the rocket and $T_w$ is the wall temperature at the location.

On the other hand, the static pressure is evaluated by the following equation:

$$P = \int_{t_r - t_a}^{t_r + t_a} \frac{P(\tau)}{P_0(\tau)} \mathrm{d}\tau \cdot P_0(t_r) \tag{3}$$

where $P(\tau)$ is the static pressure at the time $t = \tau (t_r - t_a \leq \tau \leq t_r + t_a)$ and $P_0(\tau)$ is the total pressure at this time. From one run to another, the shock tunnel used in this experiment cannot reproduce the same exact flow conditions such as the total pressure. $P_0(t_r)$ in Eq. (3) is chosen as a mean value of 4 MPa during the time-averaged period in the present experiment, and $t_r$ is the time when the pressure takes a value of $P_0(t_r)$. The static pressure is averaged in time between $t_r - t_a$ and $t_r + t_a$.

## Results and Discussion

### Distributions of Heat-Transfer Coefficient and Static Pressure

Figures 4 and 5 show the streamwise distributions of heat-transfer coefficient and static pressure for several values of the circumferential angle $\theta$ in the cases of hemisphere and conical booster noses, respectively. The horizontal axis is the axial length normalized by the main body diameter $D$, and the vertical axis shows either heat-transfer coefficient or static pressure, both of which are normalized by their undisturbed experimental values, $H_u$ and $P_u$, respectively.

The heat-transfer coefficient is nearly constant at $X/D \leq -1.1$. This value agrees with that without the booster, that is, the aerothermal effect of interaction is negligible here. Furthermore, these values show good agreement with the theoretical heat-flux value on a flat plate in the state of laminar boundary layer as predicted by Eckert's undisturbed flat-plate theory, as shown in Fig. 6. This agreement indicates that this region has a laminar boundary layer. Furthermore, streamwise heat-flux distribution along the main rocket surface without a booster, which was acquired experimentally in our laboratory, is almost flat and not increasing toward downstream. This distribution also ensures that the upstream undisturbed flow state is laminar.

To clarify the characteristic features of interaction, the results for the case of hemisphere nose at $\theta = 20$ deg will be explained in detail in the following paragraphs, referring to the analyses made in

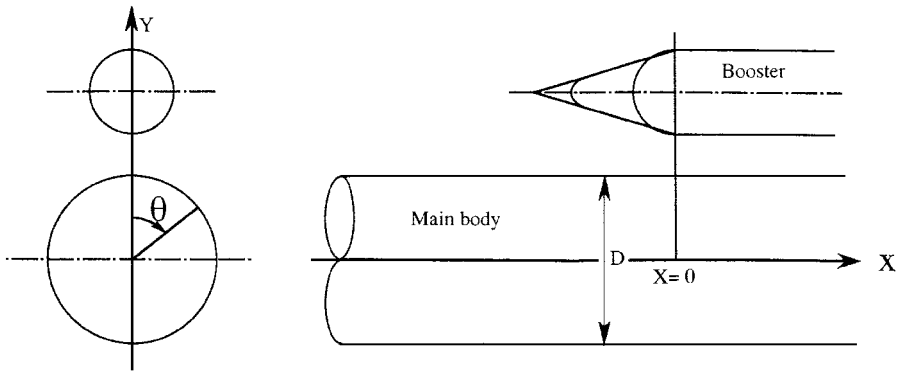


**Fig. 3 Coordinate system.**

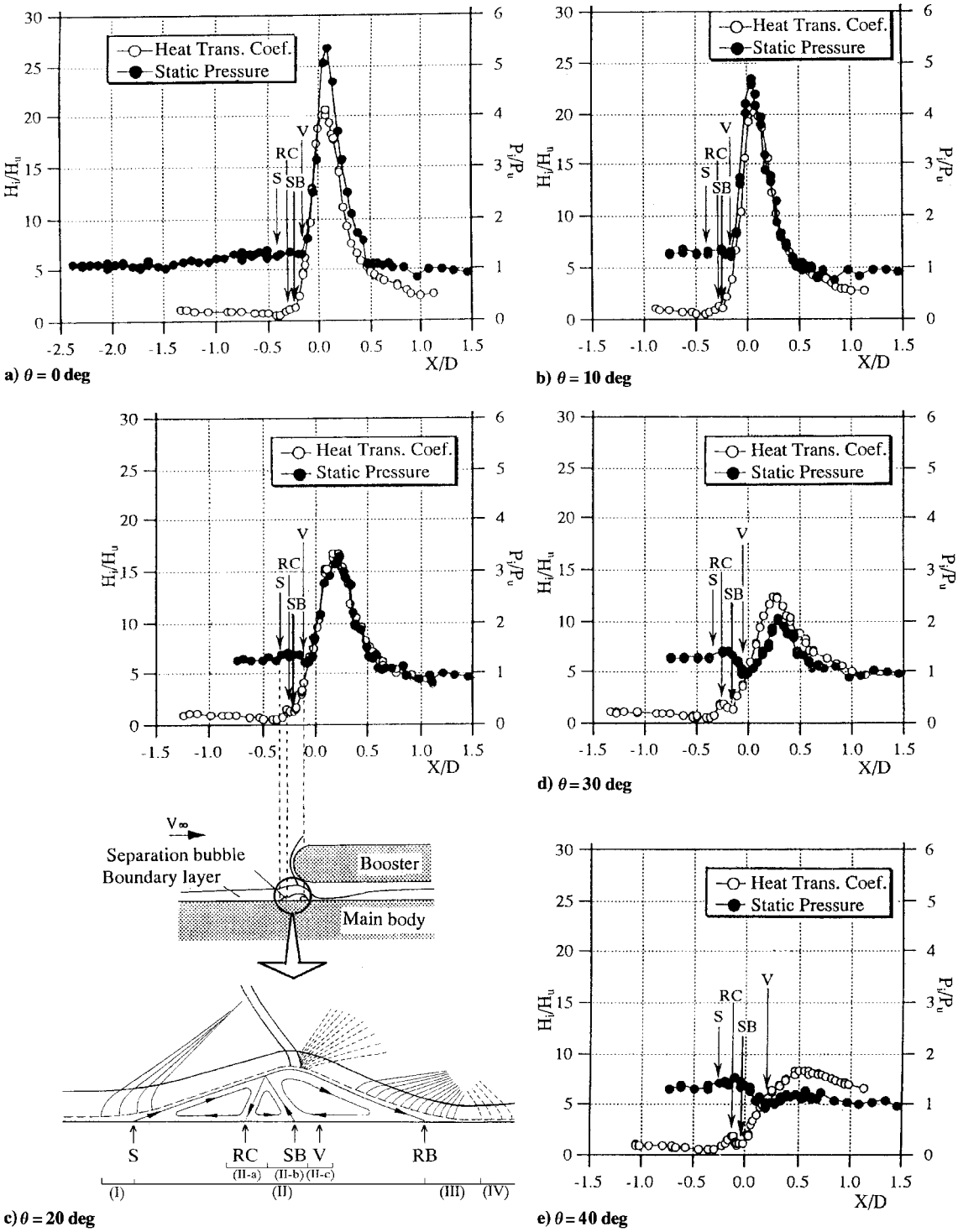


**Fig. 4 Distributions of heat-transfer coefficient and pressure on main body for hemisphere booster nose: RB, reattachment of boundary layer; RC, reattachment of flow between forward two recirculations in separation bubble; S, separation of boundary layer; SB, secondary separation between downward two recirculations in separation bubble; and V, primary recirculation.**

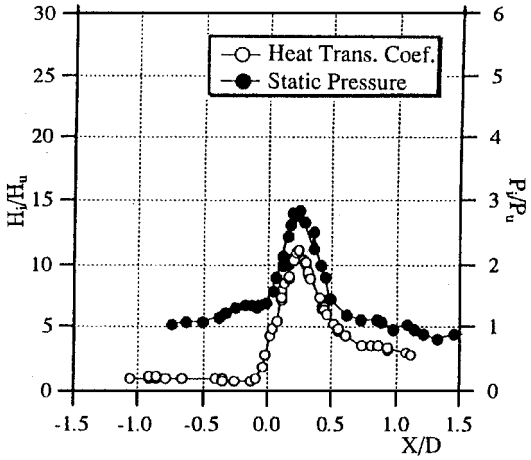


a) $\theta = 0$ deg

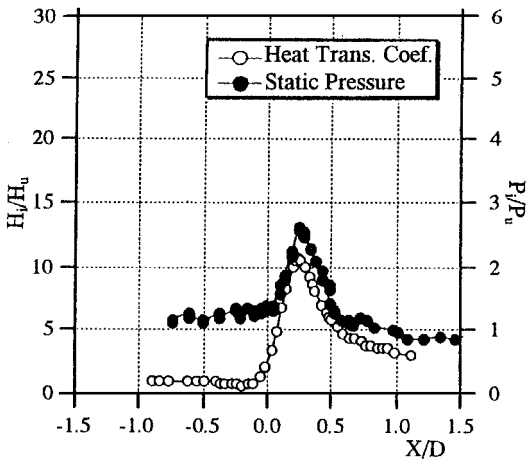


b) $\theta = 10$ deg

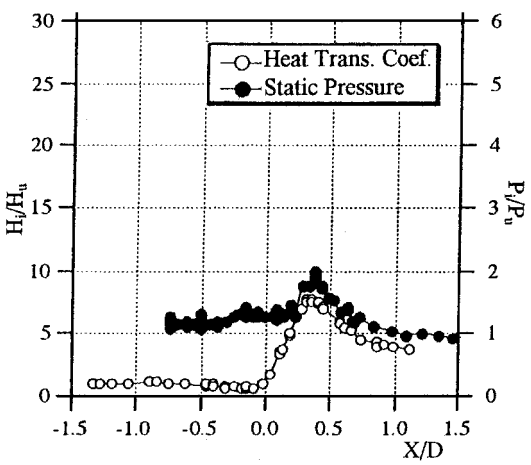


c) $\theta = 20$ deg

**Fig. 5 Distributions of heat-transfer coefficient and pressure on main body for conical booster nose.**

Refs. 3 and 7 (see Fig. 4c). In this case the interacted region can be divided into four areas: regions of (I) upstream weak compression, (II) separation, (III) reattachment and downstream compression, and (IV) expansion. The separation region (II) could consist of three distinct areas: (II-a) region with peaks of both heat flux and pressure, (II-b) region where heat flux decreases, and (II-c) region where pressure decreases. This classification is shown as a schematic view in Fig. 4.

*Region (I): Upstream Weak Compression Region*

An increase in pressure caused by shock impingement propagates upstream through the subsonic part of the boundary layer.

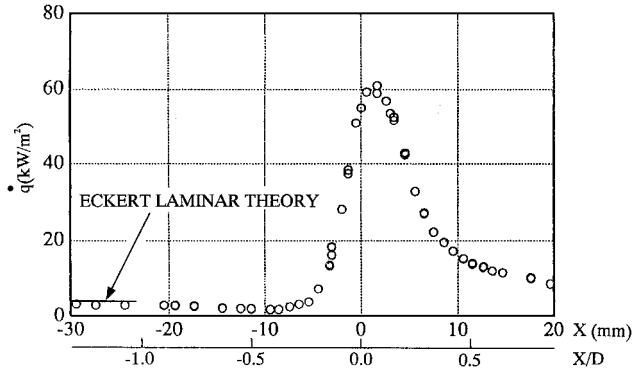


**Fig. 6 Heat-flux measurement at $\theta = 0$ deg, compared with Eckert theory.**

Then the boundary layer becomes thicker, and weak compression waves yield. The boundary layer does not separate from the surface here in this region. Consequently, static pressure gradually increases with $X$, and the heat-transfer coefficient slightly decreases, which are observed at $-1.5 \le X/D \le -0.4$ at $\theta = 0$ deg in Fig. 4a. Furthermore the heat-transfer coefficient reaches a minimum value at $X/D = -0.4$, which corresponds to $X/D = -0.35$ at a larger circumferential angle of $\theta = 20$ deg in Fig. 4c.

*Region (II): Separation Region*

Downstream of region (I), a strong adverse-pressure gradient occurs caused by a large increase in pressure. This gradient leads to boundary-layer separation shown at $X/D = -0.35$, denoted by $S$ in Fig. 4c. Pressure increase is observed at $-0.35 \le X/D \le -0.15$. Inside the separation region the following characteristic features are observed. Both distributions of heat-transfer coefficient and static pressure have their first short peaks at $X/D = -0.25$, denoted by RC in Fig. 4c. Then at $X/D = -0.2$, the heat-transfer coefficient has a minimum value, denoted by SB. The static pressure also reaches a minimum value at $X/D = -0.1$, denoted by V in the same figure. This complicated distribution is presumably because of three consecutive recirculating flows produced inside a separation bubble as shown in the schematic view of Fig. 4. That is, the first peak RC occurs as a result of the reattachment of the flow between the forward two cells. The minimum value for heat-transfer coefficient at point SB is produced by the secondary separation between the downward two recirculated cells, and the minimum value of pressure at point V occurs near the most downstream recirculating flow.

In summary, streamwise heat flux and pressure distributions along the main rocket surface with a booster show separation. The flow in this region is considered to be turbulent as well as in subsequent regions (III) and (IV). The boundary-layer state in these regions will be confirmed to be turbulent in the correlation data between peak heat-transfer coefficient and peak static pressure, which will be discussed later in the final paragraph of "Results and Discussion."

*Region (III): Reattachment and Downstream Compression Region*

Both the heat-transfer coefficient and the static pressure increase suddenly at $X/D = -0.05$ after regions (I) and (II). This phenomenon is explained as follows. The boundary layer once lifted from the wall because of a separation bubble comes back toward the wall and reattaches it. This motion of reattachment makes the boundary layer thinner, so that the temperature and velocity gradients increase at the wall, leading to a large heat-transfer coefficient. Moreover, because reattached flow vectors have to be deflected into the direction parallel to the model surface, compression waves are generated above the reattachment point. These waves cause the large increase in pressure.

*Region (IV): Expansion Region*

After reaching their peak values, the heat-transfer coefficient and the static pressure are forced to decrease by the expansion waves generated from the shoulder of the booster. Incidentally, the heat-transfer coefficient and the static pressure start to decrease at the same location.

These features are also seen in the remaining figures of Fig. 4. Comparing Figs. 4a–4e, the separation region observed over $-0.35 \leq X/D \leq -0.05$ in Fig. 4c is enlarged in Figs. 4d and 4e and reduced in Figs. 4a and 4b. The short peaks in region (II), denoted by RC in Fig. 4, become more pronounced as $\theta$ increases.

On the other hand, for the case of conical booster nose discussions on the main features are based on the results at $\theta = 20$ deg, shown in Fig. 5c. Comparing Fig. 4c with Fig. 5c, upstream of the major peaks the heat flux and the pressure have simpler distributions than the case of the hemisphere nose. Furthermore, by comparing Fig. 4a with Fig. 5a at $\theta = 0$ deg, it can be seen that an increase in pressure caused by the interaction clearly extends further upstream in the hemisphere nose case. These differences can be explained by the fact that the hemisphere booster nose produces a stronger bow shock wave than the conical one.

The data for the case of the hemisphere-cone nose are not shown here in detail because the distributions of heat flux and pressure were basically similar to those of the conical nose case. However, correlated plots between heat-transfer coefficient and static pressure will be shown later.

#### Visualization of the Surface Flow

In addition to the measurements just mentioned, flow patterns were visualized in the shock tunnel to interpret the data of heat-transfer coefficient and static pressure better. The oil-flow method was employed to observe the streamlines along the main body. In addition, schlieren method was also utilized to visualize the flowfield. The flow visualization results are shown in Fig. 7 for the case of the hemisphere booster nose. The oil-flow pattern in the upstream shows parallel streamlines, which are then turned away into the circumferential direction in front of the booster. These turning points make the line S1 on this figure, which corresponds to the point S denoted in Fig. 4. From this agreement, this point S is confirmed to be the separation point. Moreover, a white thick line seen in front of the shock impingement location, denoted by S2 in Fig. 7, also corresponds to the secondary separation inside the separation bubble, denoted by SB in Fig. 4.

The contour lines of heat-transfer coefficient and static pressure over the main body surface for the hemisphere nose case are shown in Fig. 8. The heat-transfer coefficient is affected by the interaction more extensively than the pressure. Because the main body model is not flat, but curved in the transverse direction, the pressure is easily damped in the circumferential direction of a cylindrical body. On the other hand, the heat-transfer coefficient depends not only on the pressure outside the boundary layer but also on the temperature gradient inside it. Therefore, the effect of the latter seems to persist even after that of the former vanishes. This phenomenon characterizes a three-dimensional interaction that is of interest in this study.

#### Correlation Between Heat-Transfer Coefficient and Static Pressure

It has been reported in Refs. 10 and 11 that in two- and three-dimensional shock-wave/boundary-layer interaction flowfields there are similar correlations between the ratios of the peak values of heat-transfer coefficient and static pressure to their values in undisturbed flow. The correlation derived from Eckert's reference method is expressed as

$$\frac{H_{i,\mathrm{pk}}}{H_u} = F \cdot \left( \frac{P_{i,\mathrm{pk}}}{P_u} \right)^n \tag{4}$$

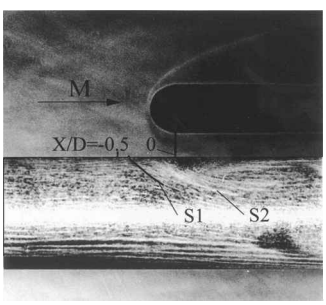


**Fig. 7 Visualization of surface flow pattern.**

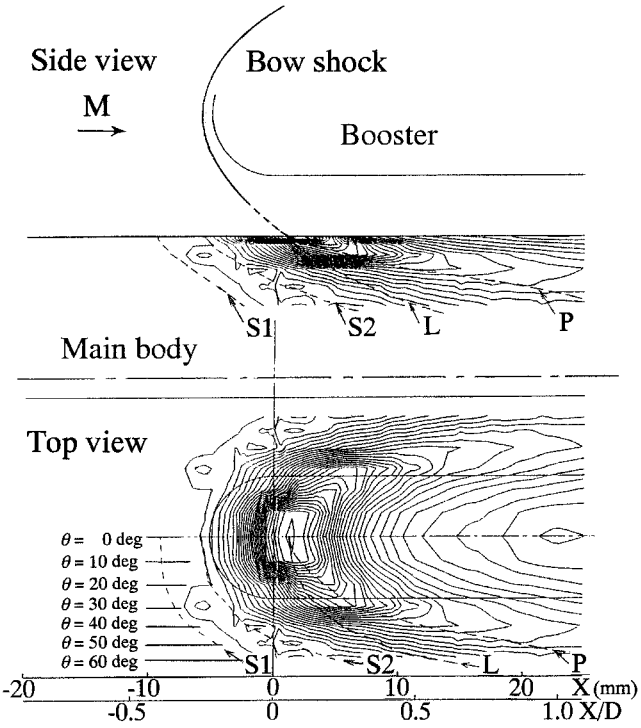


**a) Heat-transfer coefficient**

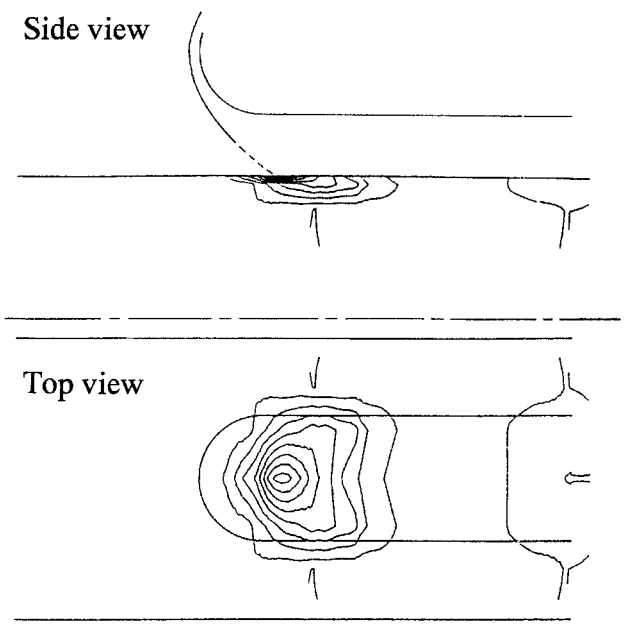


**b) Static pressure**

**Fig. 8 Contours of heat-transfer coefficient and static pressure on the surface main body: L, geometrical cross line of bow shock and main body; P, peak at each $\theta$; S1, primary separation; and S2, secondary separation.**

where $n = 0.7$ for laminar interaction, $n = 0.8$ for turbulent interaction, and $F = 1$, which were obtained by curve-fitting the experimental data. In laminar/turbulent interaction, where the laminar oncoming flow is tripped by the shock impingement and become turbulent in the downstream, the heat-transfer coefficient ratio takes a much higher value for the same pressure ratio than laminar/laminar or turbulent/turbulent interactions. Figure 9, cited from Ref. 11, shows the comparisons of the present experimental data with existing data for three-dimensional laminar/turbulent and two-dimensional laminar/laminar interactions.

All data from the present experiment take higher values than previously published data. Here we should note that most of the existing data were acquired with thin-skin thermocouples as mentioned in

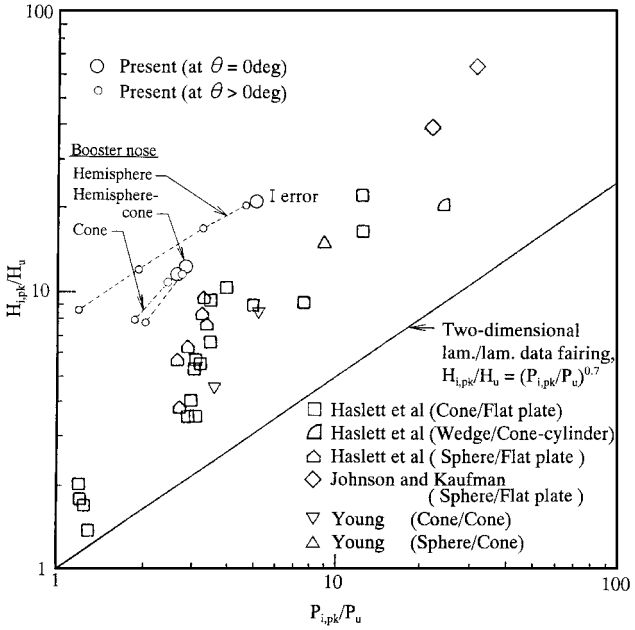


**Fig. 9 Three-dimensional laminar peak interaction heating correlation with measured pressure data: original (after Hung[11]).**

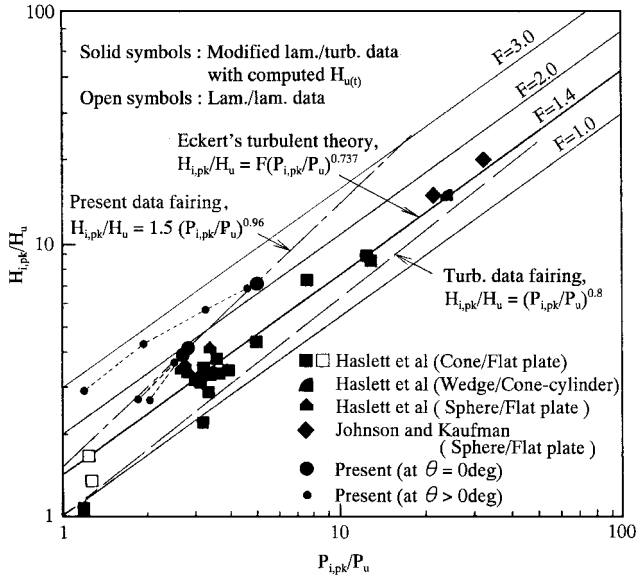


**Fig. 10 Three-dimensional laminar peak interaction heating correlation with measured pressure data: corrected (after Hung[11]).**

Ref. 11. These sensors introduce relatively large errors in data at the location at which a large temperature gradient exists along the substrate surface. In contrast, thin-film resistance thermometers employed in the present experiment have about one-order smaller errors of thermal conduction than thin-skin thermocouples. Moreover, the sensitivity of thin-film gauges to the wall temperature change is about two order higher than that of thermocouples. On the other hand, the time response of thin-film resistance thermometers, which is sub-microsecond, is the same order as that of thermocouples. Therefore, the present data should have better accuracy than the previous data.

The present heat-transfer data uncertainties are mainly composed of the uncertainties in the following four sources: 1) the temperature dependence of the gauge base substrate properties $(\rho c\kappa)^{0.5}$ ($\leq$9.5%), where $\rho$, $c$, and $\kappa$ is the density, the specific heat, and the thermal conductivity of the gauge base substrate (Pyrex type 7740, Corning), respectively; 2) the thermal properties of the gauge base substrate ($\pm$3.5%); 3) the data recording system with constant current circuits ($\pm$1%); and 4) the gauge calibration ($\pm$0.1%). As a result, the maximum possible error becomes $\pm$10.2%.

Regarding the first error source just mentioned, $(\rho c\kappa)^{0.5}$, we examined five data measured independently by several researchers. Among them, the maximum value of $(\rho c\kappa)^{0.5}$ was about 10% higher than the value at 295 K, where the maximum temperature rise in the gauge was about 35 K within a tunnel duration time of about 35 ms. The other effects of particle erosion and the curvature and the thickness of the gauge base substrate are considered to be negligible in the flowfield of this study. In the present data reduction the thermal property has been assumed to be constant for simplicity. Therefore, taking into account the effect of temperature change in the data reduction, the heat-transfer coefficient level is estimated to increase by about 10%, which is shown as an I bar in the figure.[13,14]

As discussed in Refs. 10 and 11, in addition to shock impingement, laminar/turbulent flow interaction is affected by boundary-layer transition, leading to extremely high values of $H_{i,\mathrm{pk}(t)}/H_{u(l)}$. Therefore the former contribution must be eliminated by taking the ratio of $H_{i,\mathrm{pk}(t)}$ to the undisturbed turbulent value of $H_{u(t)}$ instead of the undisturbed laminar value of $H_{u(l)}$. By doing this, reasonable comparison can be made with other types of interaction. The data thus modified are being added to the data from Ref. 11 in Fig. 10, where $H_{u(t)}$ is computed with Eckert's reference method because no measured data are available. Moreover, theoretical turbulent predictions of Eq. (4) with $n = 0.737$ and $F = 1.0$, 1.4, and 2.0, which are introduced in Ref. 11, are also shown here for comparison.

Based upon the already mentioned modification method, we fit data obtained in this study to the correlation (4). This yields the correlation parameters $n = 0.96$ and $F = 1.5$. These values are larger than the previously reported ones[11]: $n = 0.737$ and $F = 1.4$. The correlation between the peak heat-transfer coefficient and peak static pressure indicates the boundary layer to be turbulent flow in the interaction region by the shock-wave impingement, and undisturbed flow is laminar as discussed in the paragraph of "Distributions of Heat-Transfer Coefficient and Static Pressure." Because relative peak heat flux to peak pressure is much higher than those for laminar/laminar and turbulent/turbulent interactions and still higher than those for laminar/fully turbulent flow interaction. In this correlation equation with the present values of parameters, the hemisphere booster nose corresponds to a higher heating rate than the other two noses. In addition, the hemisphere-cone nose takes a closer value to the conical nose. Furthermore, if we take into account the circumferential distributions of heat-transfer coefficient and static pressure, the correlation function can hold in a wider region by increasing $F$ up to 3.0 while keeping $n$ at 0.737. The peak values of the heat-transfer coefficient and the static pressure at each circumferential angle are indicated as small circles in Fig. 10. Selecting $F$ as 3.0 might be more practical in the aerothermal design of a multiple component vehicle. These data show that a more severe aerothermal environment than what has always been considered may exist at least in the interaction flows like the present one.

## Conclusions

A shock-tunnel experiment has been conducted to study the interaction of a boundary layer developed along a rocket with a bow shock generated by a booster. Three configurations of booster nose were employed to change the strength of the bow shock: hemisphere, cone, and hemisphere-cone. Distributions of heat flux and static pressure were measured along the rocket surface in order to examine the characteristics of the interaction region and correlate both peak values. Furthermore, the three-dimensional shock/boundary-layer interacting flowfield was also visualized by the oil-flow method and the schlieren photography to help understand the data of heat flux and static pressure. From these results, the following conclusions were drawn:

1) The heat flux measured at the locations far upstream from the shock impinging point shows good agreement with the theoretical value on a flat plate in the state of laminar boundary layer by Eckert's undisturbed flat-plate theory, which indicates that this region has a laminar boundary layer.

2) In the case of hemisphere booster nose, both distributions of heat flux and static pressure have their first short peaks. Further downstream, heat flux reaches a minimum value, and so does static

pressure. This distribution is considered to be caused by three consecutive recirculating flows produced inside a separation bubble, that is, the first peak will occur as a result of the reattachment of the flow between the forward two cells. This peak becomes more pronounced as the circumferential angle $\theta$ increases. The minimum value for heat flux is produced by the secondary separation between the downward two recirculated cells, which was confirmed by oil-flow visualization. Furthermore, the minimum value of static pressure at the surface will be created near the most downstream recirculating flow.

3) For the case of conical booster nose, heat flux and static pressure have simpler distributions just upstream of the major peaks. Moreover, the increase in pressure because of interaction clearly extends further upstream for the hemisphere nose case than for the conical case. The differences between the two cases can be explained by the fact that the hemisphere booster nose produces a stronger bow shock wave than the conical one. For the case of hemisphere-cone nose, the distributions of heat flux and static pressure were basically similar to those for the conical nose case.

4) Heat flux is affected by the interaction more extensively than static pressure. Because the main body model is not flat, but curved in the transverse direction, static pressure is easily damped in the circumferential direction of a cylindrical body. On the other hand, heat flux depends not only on static pressure outside the boundary layer but also on the temperature gradient inside it. Therefore the effect of the latter seems to persist even after that of the former vanishes. This phenomenon characterizes a three-dimensional interaction, which is of interest in this study.

5) More accurate data of heat flux were acquired than the previously reported data. This is because the present data were obtained with thin-film resistance thermometers that have smaller thermal conduction errors than thin-skin thermocouples. In the correlation between heat-transfer coefficient and static pressure, using the equation derived from Eckert's reference method, all of the present data take higher values than the previously reported data on laminar/turbulent flow interaction, where the laminar oncoming flow is tripped by the shock impingement and become turbulent in the downstream. By eliminating the effect of boundary-layer transition from the present data, the correlation parameters $n$ and $F$ take the values of 0.96 and 1.5, respectively. These values are larger than the previously reported ones: $n = 0.737$ and $F = 1.4$. From these data the flow in the interaction region is considered to be turbulent, and undisturbed flow is laminar. Furthermore, if we take into account the circumferential distributions of heat flux and static pressure, the correlation function holds in a wider region by increasing $F$ up to 3.0 while keeping $n$ at 0.737. These data show that more severe aerothermal environment than what has always been considered so far exists, at least in the interaction flows like the present one.

## References

[1] Liepmann, H. W., Roshko, A., and Dhawan, S., "On Reflection of Shock Waves from Boundary Layers," NACA TN 2334, April 1951.

[2] Bogdonoff, S. M., and Kepler, C. E., "Separation of a Supersonic Turbulent Boundary Layer," *Journal of the Aerospace Sciences*, Vol. 22, No. 6, 1955, pp. 414–424.

[3] Lees, L., and Reeves, B. L., "Supersonic Separated and Reattaching Laminar Flows: I. General Theory and Application to Adiabatic Boundary-Layer/Shock-Wave Interactions," *AIAA Journal*, Vol. 2, No. 11, 1964, pp. 1907–1920.

[4] Garrison, T. J., Settles, G. S., Narayanswami, N., and Knights, D. D., "Structure of Crossing-Shock-Wave/Turbulent-Boundary-Layer Interactions," *AIAA Journal*, Vol. 31, No. 12, 1993, pp. 2204–2211.

[5] Holden, M. S., "Shock Wave-Turbulent Boundary Layer Interaction in Hypersonic Flow," AIAA Paper 77-45, Jan. 1977.

[6] Adamson, T. C., Jr., and Messiter, A. F., "Analysis of Two-Dimensional Interactions Between Shock Waves and Boundary Layers," *Annual Review of Fluid Mechanics*, Vol. 12, 1980, pp. 103–138.

[7] Delery, J., Marvin, J. G., and Reshotko, E., "Shock-Wave Boundary Layer Interactions," AG-280, AGARD, Feb. 1986.

[8] Aso, S., and Tan, A., "The Structure of Aerodynamic Heating in Three-Dimensional Shock Wave/Turbulent Boundary Layer Interactions Induced by Sharp and Blunt Fins," AIAA Paper 89-1854, June 1989.

[9] Kussoy, M. I., and Horstman, K. C., "Hypersonic Crossing Shock-Wave/Turbulent-Boundary Layer Interactions," *AIAA Journal*, Vol. 31, No. 12, 1993, pp. 2197–2203.

[10] Hung, F. T., Greenschlag, S. N., and Scottoline, C. A., "Shock-Wave-Boundary-Layer Interaction Effects on Aerodynamic Heating," *Journal of Spacecraft and Rockets*, Vol. 14, No. 1, 1977, pp. 25–31.

[11] Hung, F. T., "Three-Dimensional Shock Wave Interference Heating Prediction," AIAA Paper 77-756, June 1977.

[12] Schultz, D. L., and Jones, T. V., "Heat-Transfer Measurements in Short-Duration Hypersonic Facilities," AG-165, AGARD, Feb. 1973.

[13] Bogdan, L., "Thermal and Electrical Properties of Thin-Film Resistance Gages Used for Heat Transfer Measurement," *AIAA Journal*, Vol. 1, No. 9, 1963, pp. 2172, 2173.

[14] Miller, III, C. G., "Comparison of Thin-Film Resistance Heat-Transfer Gages with Thin-Skin Transient Calorimeter Gages in Conventional Hypersonic Wind Tunnels," NASA TM-83197, Dec. 1981.

T. C. Lin
*Associate Editor*